Cold heavy oil reservoir characterization: wormhole modeling and seismic responses

Xiaoqin Cui, Laurence R. Lines and Edward S. Krebes

ABSTRACT

Wormholes form fractural networks leading to increased reservoir permeability in the cold heavy oil production with sand (CHOPS). We extend ageneralized homogeneous approach to present an algorithm of the finite difference scheme with the fracture parameters, modeling the wormholes of CHOPS and the recorded synthetic seismograms from wormholes based on the non-welded contact theory (Schoenberg, 1980). This paper illustrates that the PP and PS seismic characters, such as amplitude, frequency, and travel time (velocity) will vary with the fractural network wormhole features. The paper exhibits that 4D seismic time-lapse technology can be used to monitor CHOPS production.

INTRODUCTION

The fact is that more than 50 percent of Canada's oil production is from heavy oil (Batzle et al., 2006), therefore, the comprehensive method of the economical recovery and production monitoring are significantly important. One of the popular heavy oil recovery methods is known as CHOPS, cold heavy oil production with sand, in which the reservoir keep the constant temperature rather than increasing temperature for the purpose of reducing heavy oil viscosity that named thermal heavy oil production. The cold production is normally suited to lowering viscosity and interfacial tension for the thin pay zone of 10 meter or less at a deeper formation of 1000 meter and more. During the cold production process, sand, oil, water, and gas are produced simultaneously by using progressive cavity pumps which generate high-porosity fractal network (channels) termed "wormholes" (Lines et al., 2008). The pattern of the grow wormholes looks like the fractal root system of a plant that has random direction of the fractures in the pay zone (Yuan et al., 1999). Based on the above the descriptions of the cold production, the volume size of a wormhole is assumed at around $200(x)*200(x)*10 \ (z)m^3$ (Figure 1). The developed wormholes induce reservoir pressure to fall below the bubble point, resulting in dissolved-gas coming out of solution to form foamy oil that derive heavy oil moving. The foamy oil can help further delineate the depletion zones or footprints to optimize drilling strategies because the foamy oil given rise the change of the gas situation and elastic velocity in the reservoir that can be illuminated the different in the seismic properties through the 4D time-lapse seismic data. (Vasheghani et al., 2008).
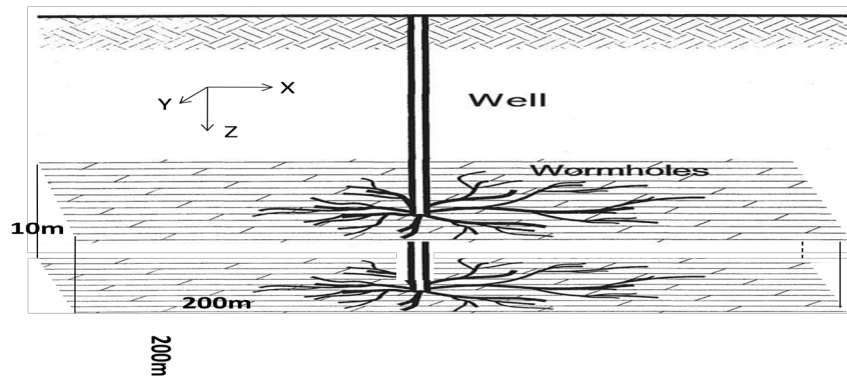
FIG. 1.A schematic of a 3D wormhole model (Modified Miller et al, 1999)

3D FINITE DIFFERENCE SCHEME FOR WORMHOLES MODELING

Through the above described the CHOPS, it is clear that the fractured network pattern form the wormhole feature having 3D geometry in the pay zone. Let us make an assumption that the x-y plane is parallel to horizontal layer and normal to the x-z plane, where x and y are horizontal axes and z is the vertical axis in Cartesian coordinate system. Thus in the x-y plane, the wormhole can be imaged as a pancake that the number of the fractures in the near central zone are less than edges of the wormhole have, and the fractures on the side lateral surface x-z plane close to the vertical one. Therefore, the elastic wave propagation through different parts of the 3D wormhole will have different responses to be recorded in a seismogram. Obviously, 3D finite difference (FD) scheme is considered to work for the wormhole forward modeling.

The traditional 3D second-order elastic wave equation is (Aki and Richards, 1980)

$$\frac{\partial^2 \boldsymbol{\varphi}}{\partial t^2} = \mathbf{A}\frac{\partial^2 \boldsymbol{\varphi}}{\partial x^2} + \mathbf{B}\frac{\partial^2 \boldsymbol{\varphi}}{\partial y^2} + \mathbf{C}\frac{\partial^2 \boldsymbol{\varphi}}{\partial z^2} + \mathbf{A}'\frac{\partial^2 \boldsymbol{\varphi}}{\partial x\,\partial y} + \mathbf{B}'\frac{\partial^2 \boldsymbol{\varphi}}{\partial x\,\partial z} + \mathbf{C}'\frac{\partial^2 \boldsymbol{\varphi}}{\partial y\,\partial z}, \qquad (1)$$

Where: $\boldsymbol{\varphi} = \begin{bmatrix} u_x \\ v_y \\ w_z \end{bmatrix}$, $\mathbf{A} = \begin{bmatrix} v_p^2 & 0 & 0 \\ 0 & v_s^2 & 0 \\ 0 & 0 & v_s^2 \end{bmatrix}$, $\mathbf{B} = \begin{bmatrix} v_p^2 & 0 & 0 \\ 0 & v_p^2 & 0 \\ 0 & 0 & v_s^2 \end{bmatrix}$, $\mathbf{C} = \begin{bmatrix} v_s^2 & 0 & 0 \\ 0 & v_s^2 & 0 \\ 0 & 0 & v_p^2 \end{bmatrix}$.

$\mathbf{A}' = \begin{bmatrix} 0 & v_p^2 - v_s^2 & 0 \\ v_p^2 - v_s^2 & 0 & 0 \\ 0 & 0 & 0 \end{bmatrix}$, $\mathbf{B}' = \begin{bmatrix} 0 & 0 & v_p^2 - v_s^2 \\ 0 & 0 & 0 \\ v_p^2 - v_s^2 & 0 & 0 \end{bmatrix}$,

$\mathbf{C}' = \begin{bmatrix} 0 & 0 & 0 \\ 0 & 0 & v_p^2 - v_s^2 \\ 0 & v_p^2 - v_s^2 & 0 \end{bmatrix}$.

Where v_p and v_s are the compressional and shear wave velocity, respectively. 3D $\boldsymbol{\varphi}$ represents x, y and z three components of wave motions, thus equation (1) can be decomposed into single x-component of thedisplacement as

$$\frac{\partial^2 u_x}{\partial t^2} = v_p^2 \left[\frac{\partial^2 u_x}{\partial x^2} + \frac{\partial^2 v_y}{\partial x\,\partial y} + \frac{\partial^2 w_z}{\partial x\,\partial z}\right] + v_s^2 \left[\frac{\partial^2 u_x}{\partial x^2} + \frac{\partial^2 u_x}{\partial y^2} - \frac{\partial^2 v_y}{\partial x\,\partial y} - \frac{\partial^2 w_z}{\partial x\,\partial z}\right],$$

As single y-component of the displacement:

$$\frac{\partial^2 v_y}{\partial t^2} = v_p^2 \left[\frac{\partial^2 u_x}{\partial x\,\partial y} + \frac{\partial^2 v_y}{\partial y^2} + \frac{\partial^2 w_z}{\partial y\,\partial z}\right] + v_s^2 \left[\frac{\partial^2 v_y}{\partial x^2} + \frac{\partial^2 v_y}{\partial z^2} - \frac{\partial^2 u_x}{\partial x\,\partial y} - \frac{\partial^2 w_z}{\partial y\,\partial z}\right],$$

And single z-component displacement as:

$$\frac{\partial^2 w_z}{\partial t^2} = v_p^2 \left[\frac{\partial^2 u_x}{\partial x\,\partial z} + \frac{\partial^2 v_y}{\partial y\,\partial z} + \frac{\partial^2 w_z}{\partial z^2}\right] + v_s^2 \left[\frac{\partial^2 w_z}{\partial x^2} + \frac{\partial^2 w_z}{\partial y^2} - \frac{\partial^2 u_x}{\partial x\,\partial z} - \frac{\partial^2 v_y}{\partial y\,\partial z}\right].$$

Define the time step as Δt, the space steps as Δx, Δy and Δz, Let Δx=Δy=Δz=h, then FD scheme for the x-component of the wave motion is as:

$$u_{x,y,z}^{t+\Delta t} = 2u_{x,y,z}^t - u_{x,y,z}^{t-\Delta t} +$$

$$(\frac{\Delta t}{h})^2 v_p^2 (u_{x+\Delta x,y,z}^t - 2u_{x,y,z}^t + u_{x-\Delta x,y,z}^t) +$$

$$(\frac{\Delta t}{h})^2 v_s^2 (u_{x,y+\Delta y,z}^t - 2u_{x,y,z}^t + u_{x,y-\Delta y,z}^t) +$$

$$(\frac{\Delta t}{h})^2 v_s^2 (u_{x,y,z+\Delta z}^t - 2u_{x,y,z}^t + u_{x,y,z-\Delta z}^t) +$$

$$\frac{1}{4}(\frac{\Delta t}{h})^2 (v_p^2 - v_s^2)(v_{x+\Delta x,y+\Delta y,z}^t - v_{x+\Delta x,y-\Delta y,z}^t - v_{x-\Delta x,y+\Delta y,z}^t + v_{x-\Delta x,y-\Delta y,z}^t) +$$

$$\frac{1}{4}(\frac{\Delta t}{h})^2 (v_p^2 - v_s^2)(w_{x+\Delta x,y,z+\Delta z}^t - w_{x+\Delta x,y,z-\Delta z}^t - w_{x-\Delta x,y,z+\Delta z}^t + w_{x-\Delta x,y,z-\Delta z}^t) \qquad (2a)$$

The FD scheme for the y-component of the wave motion is

$$v_{x,y,z}^{t+\Delta t} = 2v_{x,y,z}^t - v_{x,y,z}^{t-\Delta t} +$$

$$(\frac{\Delta t}{h})^2 v_p^2 (v_{x,y+\Delta y,z}^t - 2v_{x,y,z}^t + v_{x,y-\Delta y,z}^t) +$$

$$(\frac{\Delta t}{h})^2 v_s^2 (v_{x+\Delta x,y,z}^t - 2v_{x,y,z}^t + v_{x-\Delta x,y,z}^t) +$$

$$(\frac{\Delta t}{h})^2 v_s^2 (v_{x,y,z+\Delta z}^t - 2v_{x,y,z}^t + v_{x,y,z-\Delta z}^t) +$$

$$\frac{1}{4}(\frac{\Delta t}{h})^2 (v_p^2 - v_s^2)(u_{x+\Delta x,y+\Delta y,z}^t - u_{x+\Delta x,y-\Delta y,z}^t - u_{x-\Delta x,y+\Delta y,z}^t + u_{x-\Delta x,y-\Delta y,z}^t) +$$

$$\frac{1}{4}(\frac{\Delta t}{h})^2 (v_p^2 - v_s^2)(w_{x,y+\Delta y,z+\Delta z}^t - w_{x,y+\Delta y,z-\Delta z}^t - w_{x,y-\Delta y,z+\Delta z}^t + w_{x,y-\Delta y,z-\Delta z}^t) \qquad (2b)$$

And FD scheme for the z-component of the wave motion is

$$w_{x,y,z}^{t+\Delta t} = 2w_{x,y,z}^{t} - w_{x,y,z}^{t-\Delta t} +$$

$$(\frac{\Delta t}{h})^2 v_p^2 (w_{x,y,z+\Delta z}^{t} - 2w_{x,y,z}^{t} + w_{x,y,z-\Delta z}^{t}) +$$

$$(\frac{\Delta t}{h})^2 v_s^2 (w_{x+\Delta x,y,z}^{t} - 2w_{x,y,z}^{t} + w_{x-\Delta x,y,z}^{t}) +$$

$$(\frac{\Delta t}{h})^2 v_s^2 (w_{x,y+\Delta y,z}^{t} - 2w_{x,y,z}^{t} + w_{x,y-\Delta y,z}^{t}) +$$

$$\frac{1}{4}(\frac{\Delta t}{h})^2 (v_p^2 - v_s^2)(u_{x+\Delta x,y,z+\Delta z}^{t} - u_{x+\Delta x,y,z-\Delta z}^{t} - u_{x-\Delta x,y,z+\Delta z}^{t} + u_{x-\Delta x,y,z-\Delta z}^{t}) +$$

$$\frac{1}{4}(\frac{\Delta t}{h})^2 (v_p^2 - v_s^2)(v_{x,y+\Delta y,z+\Delta z}^{t} - v_{x,y+\Delta y,z-\Delta z}^{t} - v_{x,y-\Delta y,z+\Delta z}^{t} + v_{x,y-\Delta y,z-\Delta z}^{t}). \qquad (2c)$$

Equations (2a-c) implies that the evaluation central point (x, y, z) in FD equation of motion involves the nearest-neighbor points (e.g. x-component: $x + \Delta x, y, z$) and the next-nearest-neighbor points (e.g. x-component: $x + \Delta x, y, z + \Delta z$). In 1982, Korn and Stockl presented a generalized homogeneous approach in which the fictitious grid points are introduced to extend one medium into the nearest-neighbor medium in order to model the SH wave propagation through a boundary. In 1999, Slawinski used the generalized homogeneous approach to do 2D finite difference modeling of SH and P-SV wave propagation in nonwelded contact media. Figure 2 shows the 2D spatial stencil of the displacement with the fictitious grid points and real grid points in the x-z plane. It very clearly shows that the fictitious grid points are located as the same points as the real grid points on both side of the interface (blue dash line). This makes it possible to obtain the expression of the displacement with real points at the interfaces, and it is not difficult to solve unknown fictitious point by using boundary conditions. Thus if a fracture exists in the 3D domain, the fractures are represented as interfaces satisfying the discontinuity of displacement and continuity traction BCs across interfaces at $(x\mp1/2, y, z)$, $(x, y\mp1/2, z)$ and $(x, y, z\mp1/2)$ respectively.
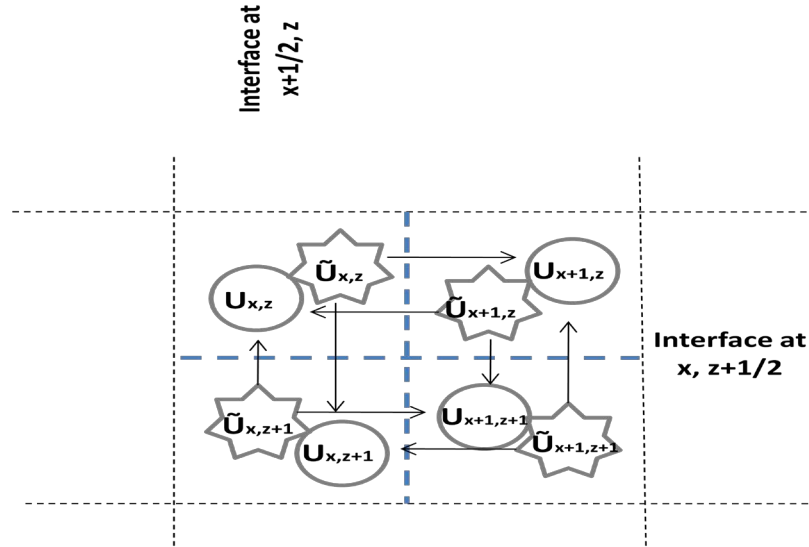
FIG. 2.2D (x-z plane) the spatial stencil of the fictitious point and real grid point with displacements.

Approximate solving the next-nearest-neighbor points by $O(\Delta x, \Delta y, \Delta z)$ Taylor expansion and replace the nearest-neighbor real grid points by fictitious points, then equation (2) yields the generalized homogeneous FD scheme of the 3D wave equation of the motion as:

$$\boldsymbol{\varphi}^{t+\Delta t}_{x,y,z} = 2\boldsymbol{\varphi}^{t}_{x,y,z} - \boldsymbol{\varphi}^{t-\Delta t}_{x,y,z} + (\frac{\Delta t}{h})^{2}\mathbf{A}(\widetilde{\boldsymbol{\varphi}}^{t}_{x+\Delta x,y,z} - 2\boldsymbol{\varphi}^{t}_{x,y,z} + \widetilde{\boldsymbol{\varphi}}^{t}_{x-\Delta x,y,z}) +$$

$$(\frac{\Delta t}{h})^{2}\mathbf{B}(\widetilde{\boldsymbol{\varphi}}^{t}_{x,y+\Delta y,z} - 2\boldsymbol{\varphi}^{t}_{x,y,z} + \widetilde{\boldsymbol{\varphi}}^{t}_{x,y-\Delta y,z}) +$$

$$(\frac{\Delta t}{h})^{2}\mathbf{C}(\widetilde{\boldsymbol{\varphi}}^{t}_{x,y,z+\Delta z} - 2\boldsymbol{\varphi}^{t}_{x,y,z} + \widetilde{\boldsymbol{\varphi}}^{t}_{x,y,z-\Delta z}). \tag{3}$$

Where $\widetilde{\boldsymbol{\varphi}}$ indicates fictitious points that correspond to real grid points. A, B and C are same as above at equation (1).

In 1980, Schoenberg gave a non-welded contact interface theory: a fracture is modeled as a non-welded contact for a linear slip interface where the particle displacements are discontinuous across the interface and the stresses are continuous across it. The particle displacements are linearly proportional to the stresses. From his pioneering work, the compliances of the fracture parameter $\boldsymbol{\eta}$ are elicited in the boundary condition. For example, if one horizontal fracture can be modeled as a horizontal interface (VTI), then

$$\boldsymbol{\varphi}^+ - \boldsymbol{\varphi}^- = \boldsymbol{\eta}\boldsymbol{\sigma}$$

$$\boldsymbol{\sigma}^- = \boldsymbol{\sigma}^+ \tag{4}$$

$$\text{Where} \boldsymbol{\varphi} = \begin{bmatrix} u_x \\ v_y \\ w_z \end{bmatrix}, \boldsymbol{\eta} = \begin{bmatrix} \eta_t & 0 & 0 \\ 0 & \eta_t & 0 \\ 0 & 0 & \eta_N \end{bmatrix}, \boldsymbol{\sigma} = \begin{bmatrix} \sigma_{xz} \\ \sigma_{yz} \\ \sigma_{zz} \end{bmatrix}.$$

$\boldsymbol{\varphi}$ represents wave motion three components x, y and z as u_x, v_y and w_z respectively. $\boldsymbol{\sigma}$ denotes normal and shear tractions of the motion. The signs of the plus and minus represent upper (left) and lower (right) medium at the interface or fracture, respectively. $\boldsymbol{\eta}$ is termed medium compliances of the fracture parameter. η_N is normal compliance for normal incident compressional wave and η_t is tangential compliance for a normal incident shear wave. η_N and η_t are orthogonal each other. In other words, η_t is parallel to the polarization of the shear wave and perpendicular to the polarization of the compressional wave, and vice-versa for η_N. The directions of the fracture and wave polarization are very critical factors and play an integral part in the forward modeling of wormholes, because the wormhole exhibits random interleaving of the horizontal and vertical fractures that have been impinged by the different wave PP and PS. Let us separate the fracture system into pure x- fracture only once the fracture's tangential compliance parallel in the x axis, and pure y-fracture meaning the tangential compliance are parallel to the y axis, therefore, the wormhole can simply decomposed into pure x-fractures and pure y- fractures in x-y plane that are projected vertical fractures in the x-z plane or y-z plane that tangential compliance takes unchanged values along z direction or thickness of the pay zone.
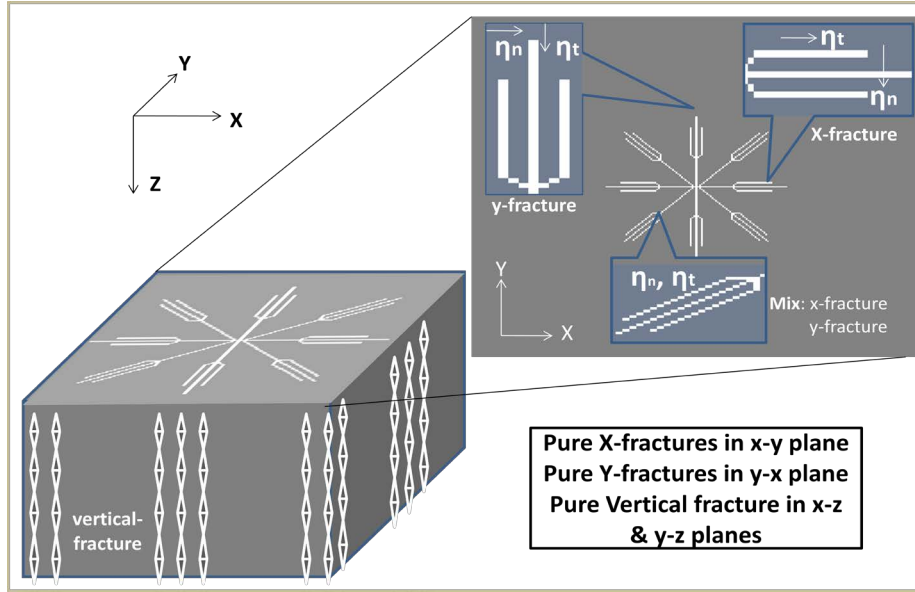
FID. 3. Wormhole schematic. The wormhole of the fractural network separates into pure x-fracture, pure y-fracture and vertical fractures.

The elastic wave can have different polarizations along the direction of the propagation. As an x-fracture case, η_t is parallel to x-z plane and x-component; y-component motions polarizations are parallel and perpendicular to tangential parameter η_t, respectively. On the other hand, for the y-fracture case, η_N is parallel to the x-z plane, and x-component and y-component displacement polarizations are parallel and perpendicular to normal compliance parameter η_N respectively. But for the z-component motion, its polarization is parallel to tangential parameter η_t in the x-fracture as well as y-fracture. The boundary conditions of the non-welded contact interface to x-fractures and y-fractures are presented as

$$\boldsymbol{\varphi}^+ - \boldsymbol{\varphi}^- = \boldsymbol{\eta}_{xy}\boldsymbol{\sigma}$$

$$\boldsymbol{\sigma}^- = \boldsymbol{\sigma}^+ \tag{5}$$

Where, $\boldsymbol{\eta}_{xy} = \begin{pmatrix} \eta x \\ \eta y \end{pmatrix}$, $\eta x = \begin{bmatrix} \eta_t & 0 & 0 \\ 0 & \eta_N & 0 \\ 0 & 0 & \eta_t \end{bmatrix}$, $\eta y = \begin{bmatrix} \eta_N & 0 & 0 \\ 0 & \eta_t & 0 \\ 0 & 0 & \eta_t \end{bmatrix}$.

$\boldsymbol{\varphi}$ and $\boldsymbol{\sigma}$ have descriptions as equation (4) above. In studying wormhole forward modeling, the fictitious point grids are employed to replace one real point grids of one side of the interface, then using BCs equation (4) and (5) to solve the fictitious point and substituted into equation (3). So it approximately generatesa generalized homogeneous finite difference scheme for 3D wave equation of motion (see detail for 2D in report 1).

Let us define the dimensionless non-weldedness parameters (Slawinski, 1999):

$$\varepsilon_x^y = \frac{\mu \eta_N}{h}, \ \varepsilon_y^y = \frac{\mu \eta_t}{h}, \ \emptyset = \frac{(\lambda + 2\mu)\eta_t}{h} \text{are for the pure y-fracture.}$$

$$\varepsilon_x^x = \frac{\mu \eta_N}{h}, \ \varepsilon_y^x = \frac{\mu \eta_t}{h}, \ \emptyset = \frac{(\lambda + 2\mu)\eta_t}{h} \text{are for the pure x-fracture.}$$

Once x-component wave motion polarized to the direction of the y axis or y-fracture, η_N contributes to it and x-component FD scheme associate with ε_x^y; whereas η_t contributes to y-component wave motion and its FD scheme is associated with ε_y^y in this time. Similarity, ε_x^x and ε_y^x are contribute to pure x-fracture. Thus the FD scheme for a 3D wormhole equation is

$$\boldsymbol{\varphi}_{x,y,z}^{t+\Delta t} = 2\boldsymbol{\varphi}_{x,y,z}^{t} - \boldsymbol{\varphi}_{x,y,z}^{t-\Delta t} + \frac{1}{\rho}\left(\frac{\Delta t}{h}\right)^2 \{\mathbf{A}_f(\boldsymbol{\varphi}_{x+\Delta x,y,z}^{t} - 2\boldsymbol{\varphi}_{x,y,z}^{t} + \boldsymbol{\varphi}_{x-\Delta x,y,z}^{t}) +$$

$$\mathbf{B}_f(\varphi_{x,y+\Delta y,z}^{t} - 2\boldsymbol{\varphi}_{x,y,z}^{t} + \boldsymbol{\varphi}_{x,y-\Delta y,z}^{t}) + \mathbf{C}_f(\boldsymbol{\varphi}_{x,y,z+\Delta z}^{t} - 2\boldsymbol{\varphi}_{x,y,z}^{t} + \boldsymbol{\varphi}_{x,y,z-\Delta z}^{t}) +$$

$$\frac{1}{4}\mathbf{D}_f\big(\boldsymbol{\varphi}_{x+\Delta x,y+\Delta y,z}^{t} - \boldsymbol{\varphi}_{x+\Delta x,y-\Delta y,z}^{t} - \boldsymbol{\varphi}_{x-\Delta x,y+\Delta y,z}^{t} + \boldsymbol{\varphi}_{x-\Delta x,y-\Delta y,z}^{t}\big) +$$

$$\frac{1}{4}\mathbf{E}_f\big(\boldsymbol{\varphi}_{x+\Delta x,y,z+\Delta z}^{t} - \boldsymbol{\varphi}_{x+\Delta x,y,z-\Delta z}^{t} - \boldsymbol{\varphi}_{x-\Delta x,y,z+\Delta z}^{t} - \boldsymbol{\varphi}_{x-\Delta x,y,z-\Delta z}^{t}\big) +$$

$$\frac{1}{4}\mathbf{F}_f\big(\boldsymbol{\varphi}_{x,y+\Delta y,z+\Delta z}^{t} - \boldsymbol{\varphi}_{x,y+\Delta y,z-\Delta z}^{t} - \boldsymbol{\varphi}_{x,y-\Delta y,z+\Delta z}^{t} + \boldsymbol{\varphi}_{x,y-\Delta y,z-\Delta z}^{t}\big)\}. \qquad (6)$$

Where,

$$\mathbf{A}_f = \begin{bmatrix} \frac{\lambda+2\mu}{1+\varnothing} & 0 & 0 \\ 0 & \frac{\mu}{1+\varepsilon_y^y} + \frac{\mu}{1+\varepsilon_y^x} & 0 \\ 0 & 0 & \frac{\mu}{1+\varepsilon_y^y} + \frac{\mu}{1+\varepsilon_x^x} \end{bmatrix}, \quad \mathbf{B}_f = \begin{bmatrix} \frac{\mu}{1+\varepsilon_x^y} + \frac{\mu}{1+\varepsilon_x^x} & 0 & 0 \\ 0 & \frac{\lambda+2\mu}{1+\varnothing} & 0 \\ 0 & 0 & \frac{\mu}{1+\varepsilon_y^y} + \frac{\mu}{1+\varepsilon_x^x} \end{bmatrix},$$

$$\mathbf{C}_f = \begin{bmatrix} \frac{\mu}{1+\varepsilon_x^y} + \frac{\mu}{1+\varepsilon_x^x} & 0 & 0 \\ 0 & \frac{\mu}{1+\varepsilon_y^y} + \frac{\mu}{1+\varepsilon_y^x} & 0 \\ 0 & 0 & \frac{\lambda+2\mu}{1+\varnothing} \end{bmatrix}, \quad \mathbf{D}_f = \begin{bmatrix} 0 & \frac{\mu}{1+\varepsilon_x^y} + \frac{\mu}{1+\varepsilon_x^x} & 0 \\ \frac{\mu}{1+\varepsilon_y^y} + \frac{\mu}{1+\varepsilon_y^x} & 0 & 0 \\ 0 & 0 & 0 \end{bmatrix},$$

$$\mathbf{E}_f = \begin{bmatrix} 0 & 0 & \frac{\lambda}{1+\varnothing} + \frac{\mu}{1+\varepsilon_x^y} + \frac{\mu}{1+\varepsilon_x^x} \\ 0 & 0 & 0 \\ \frac{\lambda}{1+\varnothing} + \frac{\mu}{1+\varepsilon_y^y} + \frac{\mu}{1+\varepsilon_x^x} & 0 & 0 \end{bmatrix},$$

$$\mathbf{F}_f = \begin{bmatrix} 0 & 0 & 0 \\ 0 & 0 & \frac{\lambda}{1+\varnothing} + \frac{\mu}{1+\varepsilon_y^y} + \frac{\mu}{1+\varepsilon_y^x} \\ 0 & \frac{\mu}{1+\varepsilon_y^y} + \frac{\mu}{1+\varepsilon_x^x} & 0 \end{bmatrix}.$$

This FD scheme for 3D wave motion with the fictitious grid points takes more physical insight into to the fracture forward modeling in that the medium and boundary conditions (BCs) are imposed explicitly. In other words, the equation of motion governs the motion outside of the discontinuity interface (fracture), but non-welded contact boundary condition is applied at the discontinuity interface.

SEISMOGRAMS AND DISCUSSION

We have implemented a Matlab code for the forward modeling of the wormhole to answer two questions:

What are the responses of physical fractural wormhole in synthetic seismogram?

How does the difference of seismic attributes vary with time for time-lapse data?

For a better understanding of the wormhole properties, it is useful to investigate numerically PP and PS synthetic seismograms from fractural network of the wormhole in the homogeneous isotropic medium. The parameters of homogeneous isotropic medium are $v_p = 2300\text{m/s}$, $v_s = 1380\text{m/s}$, $\rho = 2.37\text{g/cm}^3$. $\mu = v_s^2 \rho$, $\lambda = (v_p^2 - v_s^2)\rho$. In

practical, it raises a question about the velocity variation with azimuth of the developed wormhole because its fractural network has formed an azimuthal anisotropic medium (TI) from the initial isotopic homogeneous medium. But the velocity changes are ignored in this wormhole study in this paper. The values of the normal and tangential compliances of the fracture parameter are 0.025 and 0.049 respectively. Figure 4 shows the mapping of the source and receivers that are above 30m of the physical wormhole feature located at 360m depth. One source is located at the central point. The size of wormhole is $201(x)*201(y)*10(z)$ m^3(Figure 1). In order to avoid the problem of the FDs edge effects, it is helpful to extend spatial grids until the effective primary wave is reflected from the fracture without the interfering coming from the four edges reflections (Lines, Slawinski and Bording, 1999). Thus the geometry has a spatial grid formation of 301x301x301, and the corresponding grid size is $\Delta x = \Delta y = \Delta z = h = 2.0$m and the time step is 0.0001ms.
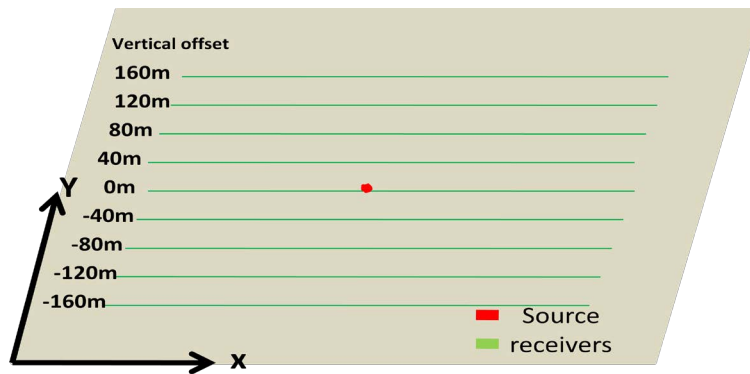
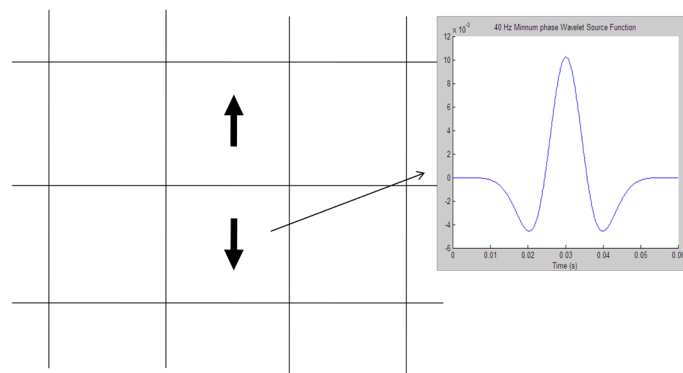FIG. 4.Shots and receivers map. Red point is a source location. Green lines are receiver lines.

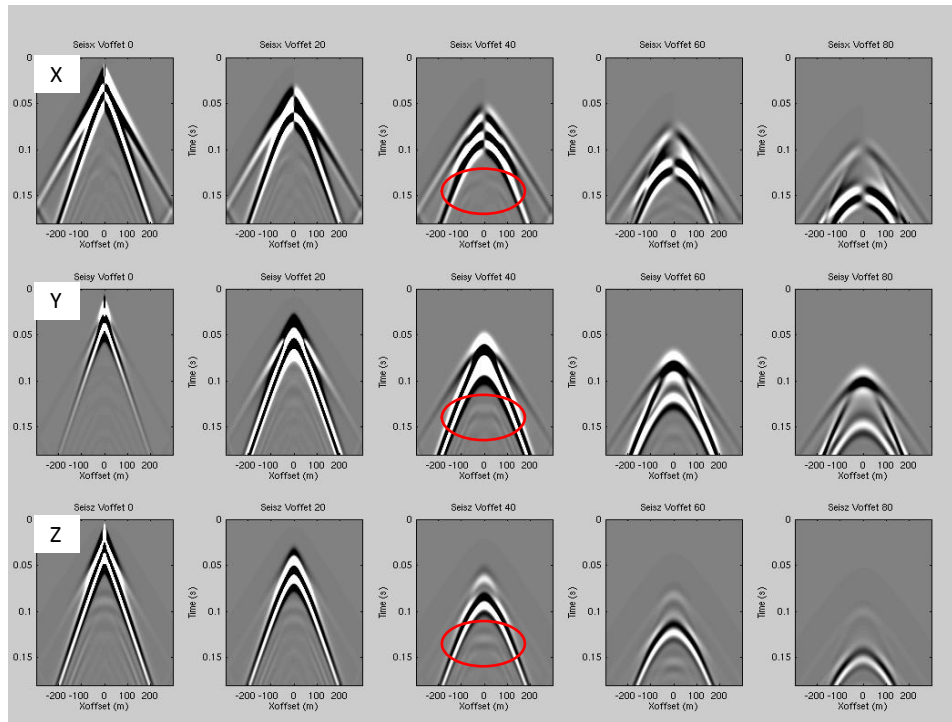FIG. 5.A normalized Ricker wave is used as the source wavelet.

FIG. 6. Three components x (top), y (middle) and z (bottom) synthetic seismograms response a wormhole.

The Ricker wavelet was introduced as a source wavelet, whichis generated from the analog expression using CREWES software as Ricker(t)=$(1-2Л^2f^2t^2)exp(-Л^2f^2t^2)$. The source wavelet is normalized so that the dominant frequency component has unit amplitude. The wavelet was multiplied with the value of positive and negative one to obtain the source wavelets for upgoing waves and downgoing waves respectively (Figure 5). For the source wavelet, the dominant frequency is 40Hz, and the breadth is t=0.06ms. Then the wavelength of primary frequency component is λ=57.5m. Figure 6 shows the three-component synthetic seismograms that record both PP and PS reflections from the wormhole feature, although there is no impedance contrast in the background medium. It illustrates different seismic characters of the wormhole at different offsets or incident angles in the three-component seismograms.

In general, when seismic wave propagates in a fractured medium, waves polarized parallel to the direction of the fracturetravel with a fast velocity, otherwise, while waves polarized perpendicular to the direction of the fracture travel with a slow velocity. Figure 7 exhibits two synthetic seismic traces extracted from seismograms of x, y and z components respectively. Trace 1 passes through a non-fractured path, and trace 2 is from fractural wormhole (pure horizontal fracture). It is clear that x and z components have similar amplitudes for trace 1 and trace 2, and the velocity of trace 2 is faster than that of trace 1 (Red line showing) because trace 2 is polarized parallel to the direction of the

fracture for both x and z components in the wormhole. Whereas trace 2 in the y component is polarized perpendicular to the direction of the fracture so that it relatively has lower velocity and weaker amplitude compared to trace 1.
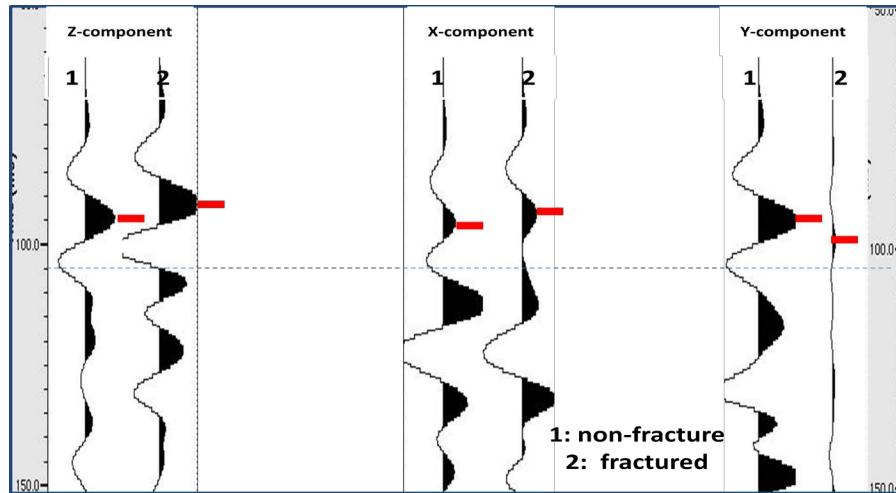

FIG. 7.Seismic trace amplitude and velocity (travel time) variations respect to the direction of the fracture. Trace 1 comes from non fracture area. Trace 2 is from fracturefeature.Trace 2 has faster velocity and relativelyhigher amplitude than the trace 1 in the x and z components (Red small lines). Trace 2 in the y component has lower velocity and amplitude than trace 1.

Seismic wave manifests frequency dispersion when it propagates into the fracture, which means that the velocity of propagating wave depends on its frequency. Figure 8 presents two traces from non-fracture area (left) and wormhole (right) respectively. The velocity is independent of frequency for the trace from non-fracture area (left). The velocity varies with frequency for the trace from fractured area
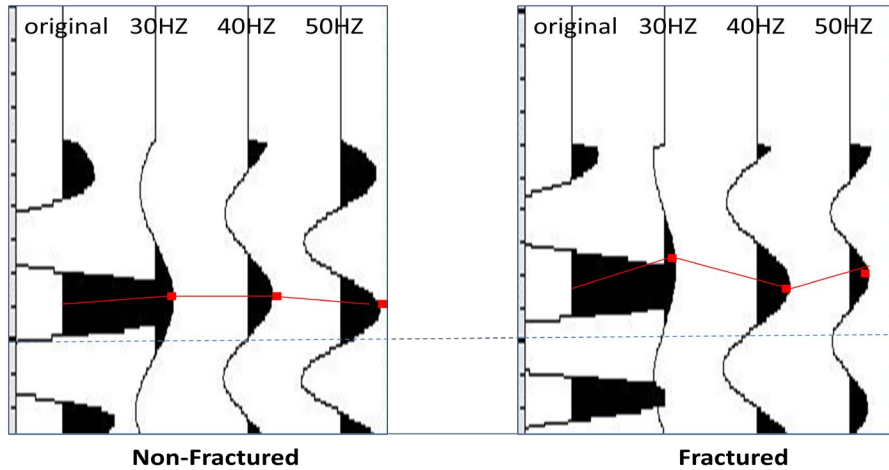
FIG. 8. Trace from the non-fracture area (left) has the velocity independent of the frequency. Trace from the fractured area (right) has frequency dispersion.

Delineation size of the depletion zones or footprints can determine optimal drilling strategy for cold production. Time-lapse seismic data can demonstrate the shape and size of wormhole base on seismic attributes in term of time slices. Figure 9a-9c show three-component records of the time-lapse data. It manifests that the size and fractural network density of developed wormhole increases with time, and trace amplitude varies with time as well. Therefore, time-lapse method is used to monitor heavy oil cold production.
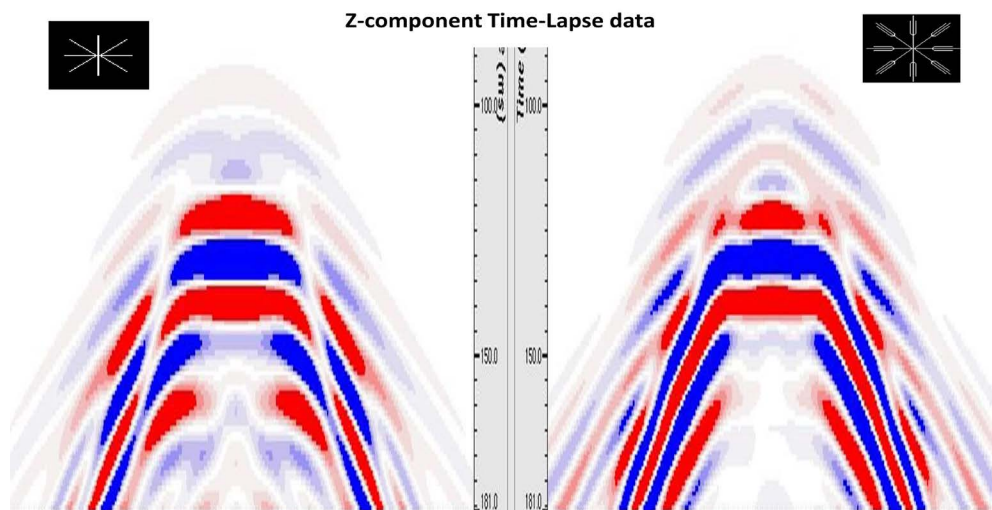

FIG. 9a.z-component synthetic records are time-lapse data. Seismic characteristics become more complex as time increases.
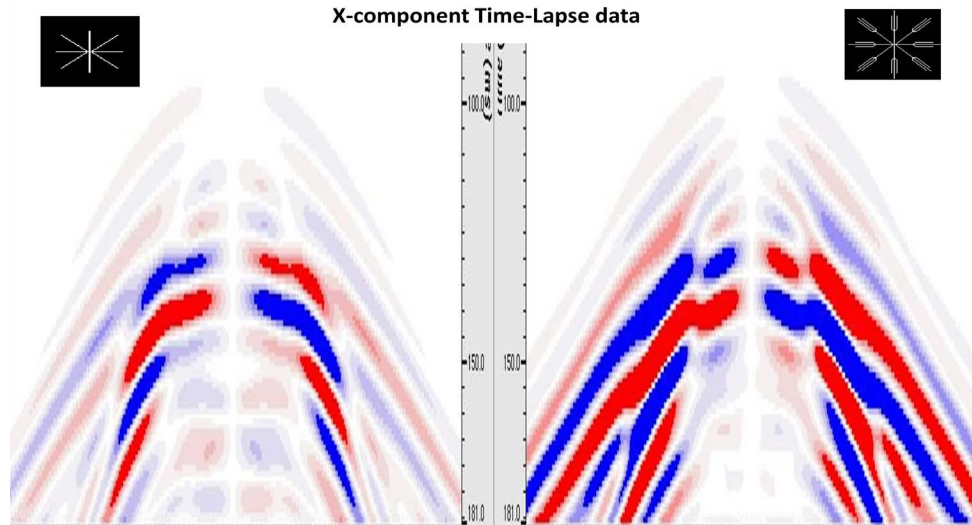
FIG. 9b x-component synthetic records are time-lapse data. Seismic characteristics become complex as time increases.
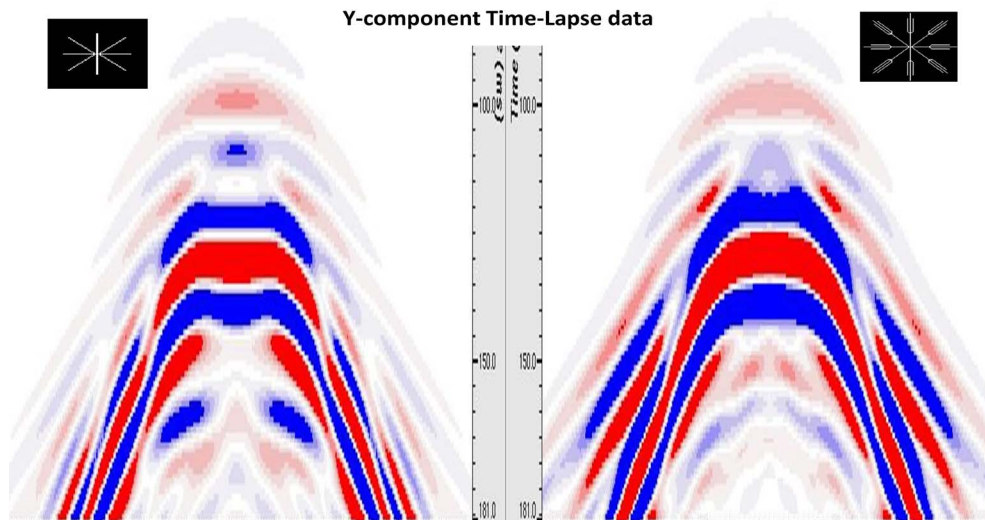

FIG. 9c.y-component synthetic records are time-lapse data. Seismic characteristics become more complex as time increases.

The time slice can identify wormhole geometrical shape. Figure 10 shows the subsurface models (black, bottom) and time slice of synthetic seismic data. Obviously, time slice of seismic data correctly matches the subsurface model. It indicates that 3D/4D seismic data can be used to avoid invalid drilling and monitor production. In figure 10b, x-component data provides additional information to learn the developed wormhole.
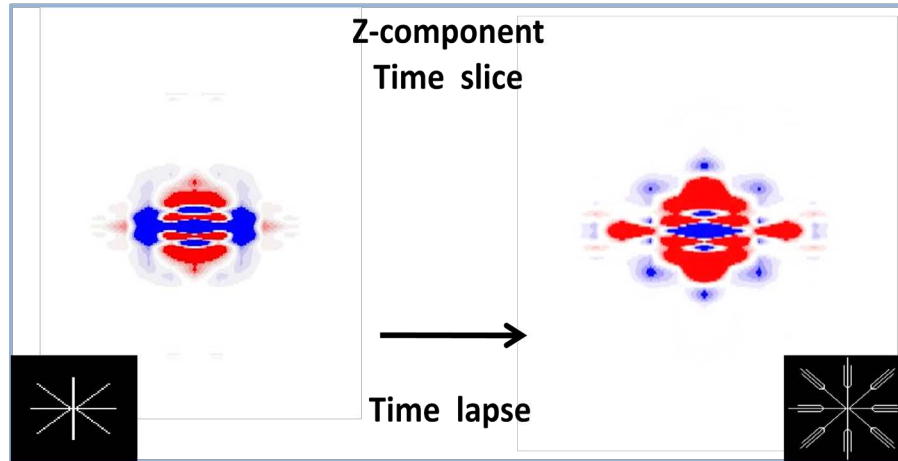
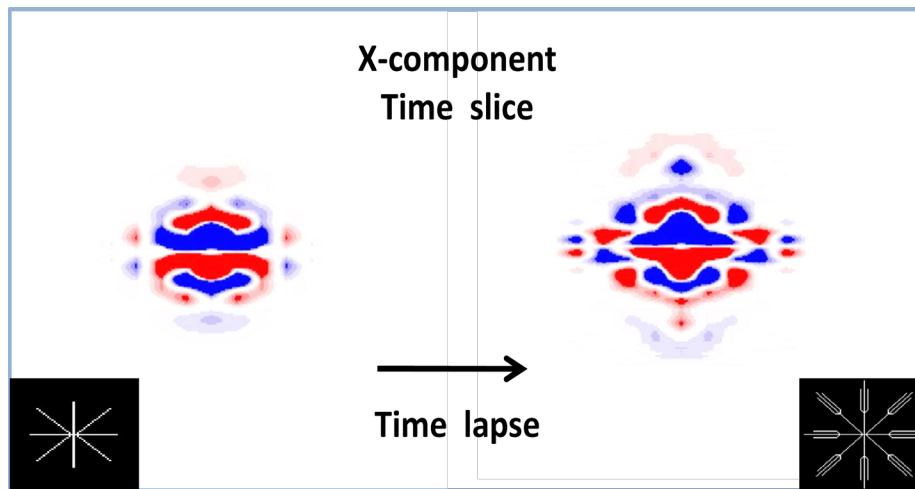FIG.10a.z-component time slices showa subsurface wormhole.

FIG.10b.x-component time slices showa subsurface wormhole.

CONCLUSION

A generalized homogeneous approach of finite difference method is extended for the 3D Seismic modeling of wormhole feature. Synthetic seismic data can be affected by wormhole demonstrating azimuthal anisotropy and frequency dispersion. Time-lapse data time slice is method to detect wormhole growth, which is used to evaluate reservoir permeability for enhancing oil & gas recovery and to avoid invalid drilling.

ACKNOWLEDGMENTS

REFERENCES

Aki, K., and Richards, P. G., 1980, Quantitative seismology, theory and methods, volume 1: W H Freeman and Co, Cambridge Press, 144 – 154.

Crampin, S., 1985, Evidence for aligned cracks in the Earth's crust: First Break, 3, no. 3, 12-15.

Coates, R.T., and Schoenberg, M., 1995, Finite-difference modeling of faults and fractures: Geophysics, 60, 1514-1526.

Hood, J. A., and Schoenberg, M., 1989, Estimation of vertical fracturing from measured elastic moduli: Journal of Geophysical Research, 94, 15,611–15,618.

Hsu, C.-J., and Schoenberg, M., 1993, Elastic waves through a simulated fractured medium: Geophysics, 58, 964–977.

Lines, L.R., Slawinski, R., and Bording, R.P., 1999, A recipe for stability of finite-difference wave-equation computations: Geophysics, 64, 967-969.

Lines, L.R., Chen, S., Daley, P.F., and Embleton, J., 2003, Seismic pursuit of wormholes: The Leading Edge, 22, 459-461.

Pyrak-Nolte, L.J., L.R. Myer., And N.G.W. Cook., 1990b, Transmission of seismic wave across single natural fracture: J. Geophys. Res. 95. 8617-8638.

Slawinski, Raphael A., and Krebes, Edward S., 2000, Finite-difference modeling of SH-wave propagation in nonwelded contact media: Geophysics, vol 67, No5.

Ruger, Andreas., 1998, Variation of P-wave reflectivity with offset and azimuth in anisotropic media: Geophysics 63, 935.

Schoenberg, M., 1980, Elastic wave behavior across linear slip interfaces:J. Acoust. Soc. Am., 68, 1516-1521.

Schoenberg, M., and Douma, J., 1988, Elastic wave propagation in media with parallel fractures and aligned cracks: Geophysical Prospecting, 36, 571-590.

Schoenberg, M., and Muir, F., 1989, A calculus for finely layered anisotropic media:Geophysics, 54, 581–589.

Schoenberg, M., and Sayers, C.M., 1995, Seismic anisotropy of fractured rock: Geophysics, 60, 204-211.

Yuan, J.Y., Tremblay, B., and Babchin, A., 1999, A wormhole network model of cold production in heavy oil: SPE Paper 54097.